A Two-Layer Wind-Driven Ocean Model in a Multiply Connected Domain with Bottom Topography

ALEXANDER KRUPITSKY* AND MARK A. CANE

Lamont-Doherty Earth Observatory of Columbia University, Palisades, New York

(Manuscript received 27 November 1995, in final form 2 April 1997)

ABSTRACT

The behavior of the solution to a two-layer wind-driven model in a multiply connected domain with bottom topography imitating the Southern Ocean is described. The abyssal layer of the model is forced by interfacial friction, crudely simulating the effect of eddies. The analysis of the low friction regime is based on the method of characteristics. It is found that characteristics in the upper layer are closed around Antarctica, while those in the lower layer are blocked by solid boundaries. The momentum input from wind in the upper layer is balanced by lateral and interfacial friction and by interfacial pressure drag. In the lower layer the momentum input from interfacial friction and interfacial pressure drag is balanced by topographic pressure drag. Thus, the total momentum input by the wind is balanced by upper-layer lateral friction and by topographic pressure drag.

In most of the numerical experiments the circulations in the two layers appear to be decoupled. The decoupling can be explained by the JEBAR term, whose magnitude decreases as interfacial friction increases. The solution tends toward the barotropic one if the interfacial friction is large enough to render the JEBAR term to be no larger than the wind stress curl term in the potential vorticity equation. The change of regimes occurs when the value of the interfacial friction coefficient κ equals $\kappa_0 = H_1 f_0 (L_y/L_x)(A/H_0)$, where f_0 is the mean value of the Coriolis parameter; L_y and L_x are the meridional and zonal domain dimensions; H_0 and H_1 are the mean depths of the ocean and of the upper layer; and A is the amplitude of topographic perturbations. Note that κ_0 does not depend on the strength of the wind stress.

The magnitude of the total transport is found to depend crucially on the efficiency of the momentum transfer from the upper to the lower layer, that is, on the ratio κ/ε, where ε is the lateral friction coefficient. If ε and κ are assumed to be proportional, the upper-layer transport and total transport vary as $\varepsilon^{-5/6}$.

1. Introduction

It is still unclear why the Antarctic Circumpolar Current (ACC) carries as much water as it does. Even one of the most detailed numerical models to date, FRAM (Fine Resolution Antarctic Model) (FRAM Group 1991, overestimates the total ACC transport by about 50% (Grose et al. 1995). Since observations show that the ACC is strongly steered by bottom relief (e.g., Gordon et al. 1978), many researchers have concentrated on topographic effects on the ACC.

Recent studies by Krupitsky and Cane (1994), Krupitsky (1995), Wang and Huang (1995), and Wang (1994) have largely completed the linear theory of barotropic currents in the circumpolar domain with bottom topography that was pioneered by Kamenkovich (1960, 1962). Two dynamically distinct situations are found. In the first, the topography is small enough for there to be closed (circumpolar) geostrophic contours (lines of constant f/H, f being the Coriolis parameter and H the depth). Since the pressure gradient cannot build up on a closed geostrophic contour, friction, no matter how small the coefficient is, must balance the wind input. The total transport varies inversely with friction (Kamenkovich 1962). In the second case the topography exceeds the critical height where closed geostrophic contours vanish. The momentum input by the wind is balanced by bottom pressure drag and the transport is independent of friction to leading order (e.g., Krupitsky and Cane 1994). The present work extends these results to a stratified ocean.

Numerical experiments have demonstrated that stratification can efficiently shield the circulation in the upper ocean from topographic effects. For example, the ACC transport in the Cox (1975) GFDL baroclinic global ocean model is 184 Sv (Sv $\equiv 10^6$ m^3 s^{-1}), but it is only 21.5 Sv in the barotropic case with the same parameters. Thus in this experiment baroclinicity leads to a more than eight-fold increase in the ACC transport.

Topographic effects on the ACC have been extensively studied using layered quasigeostrophic models

* Current affiliation: Woods Hole Oceanographic Institution, Woods Hole, Massachusetts.

Corresponding author address: Dr. Alexander Krupitsky, Department of Physical Oceanography, Woods Hole Oceanographic Institution, MS #21, Woods Hole, MA 02543.
E-mail: sasha@dragon.whoi.edu

(e.g., McWilliams et al. 1978; Wolff and Olbers 1989; Wolff et al. 1990; Trenguier and McWilliams 1990; Wolff et al. 1991). These studies have shown that the transport in the abyssal layer can be very strongly affected by topography while the transport in the rest of water column is relatively robust.

A critical issue facing a researcher intending to tackle a baroclinic problem analytically is how to force the layers insulated from the direct action of the wind. In layer models, in the absence of vertical viscosity the steady motion in abyssal layers is entirely due to eddies (Harrison 1979). The same is true of level models. For example, Stevens and Ivchenko (1994, unpublished manuscript) interpreted the downward penetration of momentum in terms of meridional density fluxes and Eliassen–Palm fluxes. Since the treatment of eddies is very complicated, most researchers employed various parameterizations and hypotheses to take the action of eddies into account implicitly. We consider the interfacial friction in our model to be a crude but useful parameterization of eddy effects.

Wang (1993) assumed that eddies homogenize potential vorticity (and therefore implicitly act as a sink or source of momentum) in the deep layers of a quasigeostrophic channel model with weak interfacial and bottom friction. Topography in his model was represented by a meridional ridge high enough to block all geostrophic contours. In the limit of small explicit friction, the barotropic part of the solution is identical to the solution of the corresponding barotropic problem, while the shear is independent of the wind and is determined by the requirement of potential vorticity homogenization in the subsurface layers.

Marshall (1995) took a continuous equivalent of the same assumption; that is,

$$f\frac{\partial p}{\partial z} = Q(\rho),$$

where ρ is the potential density and Q is chosen to be a linear function, which implies exponential variation of density with depth. The problem was solved following characteristics, which were shown to lie between the f/H contours of a homogeneous ocean and f contours of a strongly stratified ocean. The ''initial'' value of surface density had to be prescribed at some longitude to determine the solution. In the limit of weak bottom currents, the ACC transport is found to be 160 Sv. The circulation consists of circumpolar flow in the upper 3 km and abyssal gyres trapped by bottom topography.

Here we will consider a two-layer wind-driven model in a doubly connected domain with bottom topography submerged in the lower layer. The lower layer is driven by interfacial friction and by interfacial pressure drag. Our primary goal is to describe the solution qualitatively and to understand the nature of the momentum balances, which determine the transport. Numerical experiments confirm our analysis. In addition, the issue of coupling between the layers is studied.

2. The model

Consider a circumpolar ocean of depth H bounded by solid boundaries Γ_N at the north and Γ_S at the south. The momentum equations for the steady circulation in a two-layer ocean are assumed to be

$$f\mathbf{k} \times \mathbf{u}_1 = -g\nabla\eta - \varepsilon\mathbf{u}_1 - \kappa(\mathbf{u}_1 - \mathbf{u}_2)/h_1 + \boldsymbol{\tau}/h_1, \quad (1)$$

$$f\mathbf{k} \times \mathbf{u}_2 = -g\nabla\eta + g'\nabla h_1 - \varepsilon\mathbf{u}_2 + \kappa(\mathbf{u}_1 - \mathbf{u}_2)/h_2, \quad (2)$$

where h_1 and h_2 are the thicknesses of the upper and lower layers respectively, $\mathbf{u}_i = (u_i, v_i)$ are the horizontal velocities in each layer, η is the surface elevation, f is the Coriolis parameter, g' is reduced gravity, and κ is the interfacial friction coefficient. Interfacial friction in the present model stands in for the effect of eddies. Lateral viscosity and horizontal divergence of the Reynolds stresses are parameterized by the Rayleigh friction terms $\varepsilon\mathbf{u}_i$.

Subtracting (2) from (1),

$$f\mathbf{k} \times (\mathbf{u}_1 - \mathbf{u}_2) = -g'\nabla h_1 + \boldsymbol{\tau}/h_1 - \lambda f(\mathbf{u}_1 - \mathbf{u}_2), \quad (3)$$

where

$$\lambda = \frac{1}{f}\left(\varepsilon + \frac{H}{h_1 h_2}\kappa\right) \quad (4)$$

is a nondimensional friction coefficient; typically $\lambda \ll 1$. The transport streamfunctions are defined as

$$\mathbf{k} \times \nabla\psi_i = \mathbf{u}_i h_i, \qquad (i = 1, 2),$$
$$\mathbf{k} \times \nabla\psi = \mathbf{u}_1 h_1 + \mathbf{u}_2 h_2. \quad (5)$$

Using (2), (3), (5) to eliminate $\mathbf{u}_2$ in (1), we obtain

$$\mathbf{u}_1 = \frac{\mathbf{k} \times \nabla\psi}{H} + \frac{h_2}{f(1 + \lambda^2)H} \times \left[\left(g'\mathbf{k} \times \Delta h_1 - \frac{\mathbf{k} \times \boldsymbol{\tau}}{h_1}\right) - \lambda\left(g'\Delta h_1 - \frac{\boldsymbol{\tau}}{h_1}\right)\right]. \quad (6)$$

Taking the curl of the vertically averaged momentum equations yields

$$\varepsilon\left[\nabla\cdot\left(\frac{1}{H}\nabla\psi\right)\right] + J\left(\psi, \frac{f}{H}\right) - \frac{g'}{2}J\left(h_1^2, \frac{1}{H}\right) = \mathrm{curl}_z\frac{\boldsymbol{\tau}}{H}. \quad (7)$$

The last term on the left of (7), known as JEBAR (joint effect of baroclinicity and relief), was first introduced by Sarkisyan and Ivanov (1971). Substituting (6) into the steady upper-layer mass conservation equation

$$\nabla\cdot(\mathbf{u}_1 h_2) = 0 \quad (8)$$

gives an equation for the interface displacement

$$J\left(\psi, \frac{h_1}{H}\right) + \frac{g'}{2} J\left(h_1^2, \frac{1 - h_1/H}{f(1 + \lambda^2)}\right) = \nabla\cdot\mu\nabla h + \nabla\cdot\left[\frac{1}{f(1 + \lambda^2)}\left(1 - \frac{h_1}{H}\right)\mathbf{k} \times \boldsymbol{\tau}\right] - \nabla\cdot\left[\frac{\lambda}{f(1 + \lambda^2)}\left(1 - \frac{h_1}{H}\right)\right], \quad (9)$$

where

$$\mu = \frac{g'\lambda h_1(1 - h_1/H)}{f(1 + \lambda^2)} \approx \frac{g'}{f^2}\left(\frac{h_1 h_2}{H}\varepsilon + \kappa\right) \quad (10)$$

is the nonlinear mixing coefficient. Notice that μ is proportional to λ in the limit $\lambda \to 0$ and is significant even for small λ. For typical parameters of this model [$g' = O(10^{-2}$ ms$^{-2})$, $h_1 = O(1$ km), $\varepsilon = O(10^{-5}$–10^{-7} s$^{-1})$, $\kappa = O(10^{-2}$–10^{-4} m s$^{-1})$], one finds $\mu = O(10^2$–10^4 m^2 s$^{-1})$. Equations (7), (9) constitute a closed system with respect to ψ and h_1.

The boundary conditions are periodicity in x with period L_x and

$$\psi|_{\Gamma_N} = 0, \qquad \psi|_{\Gamma_S} = T \quad (11)$$

$$u_{1,n}|_{\Gamma_N + \Gamma_S} = 0, \quad (12)$$

where the subscript n denotes the component of velocity normal to the solid boundary. Here, T is the total transport, which can be found by integrating the vertically averaged zonal momentum equation

$$\int_0^{L_x}\left[\frac{f}{H}\frac{\partial\psi}{\partial x} - \frac{g'}{2H}\frac{\partial h_1^2}{\partial x} + \frac{\boldsymbol{\tau}^{\mathbf{x}}}{H} + \frac{\varepsilon}{H}\frac{\partial\psi}{\partial y}\right] dx = 0 \quad (13)$$

along any latitude line unobstructed by land (Kamenkovich 1962).

Taking the curl of the steady vertically averaged momentum equations within each layer yields equations for ψ_1 and ψ_2:

$$J\left(\frac{f}{h_1}, \psi_1\right) = \nabla\cdot\left(\frac{\varepsilon}{h_1}\nabla\psi_1\right) + \nabla\cdot\left[\frac{\kappa}{h_1}\left(\frac{\nabla\psi_1}{h_1} - \frac{\nabla\psi_2}{h_2}\right)\right] - \mathrm{curl}_z\frac{\boldsymbol{\tau}}{h_1} \quad (14)$$

$$J\left(\frac{f}{h_1}, \psi_2\right) = \nabla\cdot\left(\frac{\varepsilon}{h_2}\nabla\psi_2\right) + \nabla\cdot\left(\frac{\kappa}{h_2^2}\nabla\psi_2\right) - \left(\nabla\cdot\frac{\kappa}{h_1 h_2}\nabla\psi_1\right). \quad (15)$$

The system (7), (9) governing the interface displacements is nonlinear and is very difficult to solve. [An unforced inviscid version of (7), (9) was considered by Salmon (1992).]

Straub (1993) hypothesized that geostrophic contours in the upper layer f/h_1 are closed whereas those in the lower layer are blocked. This can be supported by the following reasoning: interface displacements are small compared to the mean thickness of the upper layer whereas the largest topographic features observed in the Southern Ocean should be able to block geostrophic contours in the lower layer. The other possibilities are that geostrophic contours are closed or blocked in both layers. (It is not plausible that geostrophic contours in the upper layer are blocked while those in the lower layer are closed.) Let us consider these possibilities assuming the existence of a stationary solution to (7), (9).

To facilitate the analysis we temporarily assume a relationship between the Rayleigh friction term and interfacial friction terms:

$$\kappa = \alpha H_1 \varepsilon, \quad (16)$$

where H_1 is the mean depth of the upper layer and α is some bounded coefficient.

It follows from (9) and (10) that for sufficiently large friction the amplitude of the upper-layer thickness perturbation is small enough to allow closed geostrophic contours in the upper layer. Those in the lower layer will be closed if topography is sufficiently high. Thus Straub's hypothesis is consistent with the equations of motion for at least some combination of model parameters. If closed geostrophic contours in the upper layer exist, the absolute values of f/h_1 equatorward of the band of closed geostrophic contours (hereafter B) are smaller than those poleward of the band. Integration of (1) around a closed contour of f/h_1 yields an integrated momentum balance

$$\oint\left[\frac{\varepsilon}{h_1}\frac{\partial\psi_1}{\partial n} + \frac{\kappa}{h_1}\left(\frac{1}{h_1}\frac{\partial\psi_1}{\partial n} - \frac{1}{h_2}\frac{\partial\psi_2}{\partial n}\right) + \frac{\tau_s}{h_1}\right] ds = 0. \quad (17)$$

Suppose for a moment that the *dependence* of interfacial pressure drag on friction is negligible; that is, the same integration contour in (17) can be used over some range of friction parameters. Then (16) and (17) imply

$$\psi_1 = O(\tau_0 L_y/\varepsilon), \quad (18)$$

where τ_0 is the amplitude of the wind stress and L_y is

the meridional scale of the domain. With increasing κ (increasing α) an increasing portion of the momentum input from wind is balanced by interfacial friction and thereby passed to the lower layer. Consequently, within band B the lower layer is forced in a formally similar manner to the wind forcing in the upper layer. Since geostrophic contours in the lower layer are blocked, (15) is qualitatively similar to barotropic problems considered by Krupitsky and Cane (1994) and Krupitsky (1995).

Consider now how the stationary solution will change with decreasing friction. The solution in the upper layer will grow as ε^{-1} within the band of closed f/h_1 lines, as shown by Kamenkovich (1962). It follows from (3) that this should be accompanied by increasing thermocline slope. With eastward wind, h_1 will be thicker at the equatorward side of the channel and thinner at the poleward one. As a result, $|f/h_1|$ will decrease in the equatorial part and increase in the polar part of B, thereby widening the range of values of f/h_1 within the band.

At the same time, with decreasing friction, $h_2 = H - h_1$ will become thinner in the equatorial part and thicker in the polar part, thereby enhancing the blockage of potential vorticity contours in the lower layer. Then it follows from the results of Krupitsky and Cane (1994) that the solution in the lower layer is independent of friction to leading order. Thus we find that the regime suggested by Straub (1993) is not only possible but holds for a wide range of parameters.

This simplified picture is somewhat altered by the *dependence* of interfacial pressure drag on friction. When ε and κ decrease, upper-layer velocity need not grow as ε^{-1} to maintain the momentum balance because interfacial pressure drag can pick up part of the slack. Therefore, upper-layer velocity increases less rapidly while increasing interfacial pressure drag provides an additional forcing for the lower layer.

To estimate the effect of interfacial pressure drag on the upper-layer transport T_1, we make use of the barotropic model analysis by Johnson and Hill (1975). For the upper layer, the role of bottom topography is played by the interface h_1. The zonal momentum balance (1) integrated over the volume of the upper layer can be written as

$$\nu R T_1 \approx F_\tau \equiv \frac{1}{L_x}\iint \tau^x \, dx \, dy, \tag{19}$$

where $\nu = \varepsilon + \kappa/H_1$ and R is the ''reduction'' factor due to nonzero correlation between surface elevation η and topography (of the interface, in this case):

$$\iint h_1 \nabla\eta \, dx \, dy \neq 0.$$

This integral represents the interfacial pressure drag. Johnson and Hill (1975) showed that

$$R \approx \frac{1}{L_x}\int_0^{L_x}\left[1 + \frac{f_0^2}{\beta^2 H_0^2}\left(\frac{\partial h_1}{\partial x}\right)^2\right] dx,$$

where H_0 is the mean ocean depth. Zonal perturbations of the interface are entirely due to the lower-layer current. To see this, note that if the lower layer is stagnant, then the interface tilts only to compensate for the tilt in the sea level, which is assumed to be a function of y only. Hence (3) implies

$$\frac{\partial h_1}{\partial x} = O\left(\frac{f_0}{g' H_2}\frac{\partial \psi_2}{\partial x}\right), \tag{20}$$

where H_1 and H_2 are the mean thicknesses of the upper and the lower layers. We thus need an estimate for the zonal gradient of the lower-layer flow ψ_2. For this argument we assume that ψ_2 is mainly driven by interfacial friction in the region of fast upper layer flow B; that is, by the last (''external'' forcing) term in (15), $F_2 = O(\kappa T_1/H_1 H_2 L_y^2)$. The gradients of ψ_2 are concentrated within the internal boundary layers of width $O(L_x(\nu/f_0)^{-1/2})$ (Krupitsky and Cane 1994). The jump across the boundary layer in ψ_2 $O(F_2 H_2 L_x L_y/f_0) = O(\kappa T_1 L_x/f_0 H_1 L_y)$ and the internal boundary layers are slanted at the angle $O(L_y/L_x)$, assuming $L_x \gg L_y$. Therefore, (20) implies

$$\frac{\partial h_1}{\partial x} = O\left[\frac{\kappa T_1}{g' L_x H_1 H_2}(\nu/f_0)^{-1/2}\right] \tag{21}$$

and

$$R = 1 + O\left[\frac{f_0^2}{\beta^2 H_0^2}\left(\frac{\partial h_1}{\partial x}\right)^2(\nu/f_0)^{1/2}\right]. \tag{22}$$

Substituting (21) in (22) yields

$$R = 1 + O\left[\left(\frac{\kappa T_1 f_0}{g'\beta L_x H_0 H_1 H_2}\right)^2(\nu/f_0)^{-1/2}\right].$$

Using (16), (19) becomes a cubic equation for T_1

$$(1 + \varepsilon^{3/2} q T_1^2)\varepsilon T_1 = F_\tau(1 + \alpha)^{-1}, \tag{23}$$

where $q = f_0^{3/2}(\alpha^{-1} g'\beta L_x H_0 H_2)^{-2}(1 + \alpha)^{-1/2}$. For sufficiently small ε the solution to (23) varies as $\varepsilon^{-5/6}$. For the parameters used in numerical experiments described below, $\varepsilon^{3/2} q T_1^2 \ll 1$, therefore one expects the rate of growth of T_1 to be between $\varepsilon^{-5/6}$ and ε^{-1}. This is in contrast to Wang (1993), who found a finite ''inviscid'' limit of the transport in all layers. Note, however, that, since Wang (1993) assumed that baroclinic instability would limit the shear growth, there is implicit dissipation in his model, even as $\varepsilon \to 0$. Equation (23) can be rewritten as

$$\hat{\varepsilon}^{5/2} q_0 \frac{\alpha^2}{(1 + \alpha)^2} T_1^3 + \hat{\varepsilon} T_1 = F_\tau,$$

where $\hat{\varepsilon} = \varepsilon(1 + \alpha)$ may be termed the total friction coefficient, and $q_0 = f_0^{3/2}(g'\beta L_x H_1 H_2)^{-2}$. It follows that

for sufficiently small $\hat{\varepsilon}$, T_1 is independent of α for large α and varies as $\alpha^{-2/3}$ for small α.

3. Numerical experiments

We seek to verify the results in a series of numerical experiments. We either integrated the time-dependent versions of (7) and (9) or solved (6), (7), and (8) directly. The two systems are equivalent but the boundary conditions are more conveniently handled in the latter. The numerical experiments were conducted for a periodic zonal channel with vertical walls on a β plane ($0 \le x \le L_x$, $0 \le y \le L_y$) centered at 60°S. We used the C-grid for space variables and the leapfrog scheme for time differencing. The forcing and model parameters were chosen as follows: $H = H_0 - A \sin(2\pi x/L_x)$, $H_0 = 4$ km, $H_1 = 1$ km, $A = 1.5$ km, $\tau^x = \tau^0 \sin(\pi y/L_y)$, $\tau^y = 0$, $\tau^0 = 10^{-4}$ m^2 s^{-2}, $L_x = 20\,000$ km, and $L_y = 1320$ km. The mean value of the Coriolis parameter is $f_0 = -1.26 \times 10^{-4}$ s^{-1} and $\beta = 1.14 \times 10^{-11}$ m^{-1} s^{-1}.

The very high topography ($A = 1.5$ km) was chosen to ensure blocking of geostrophic contours in the lower layer. It allows us to compare the true behavior of the solution with the estimate of the previous section far from the quasigeostrophic limit.

Most experiments were conducted on a $4° \times 2°$ grid. In the first series of experiments we set $\kappa = \varepsilon H_1$, that is, $\alpha = 1$. For the smallest values of ε and κ that we tried on the $4° \times 2°$ grid ($\varepsilon < 2 \times 10^{-7}$ s^{-1}, $\kappa < 2 \times 10^{-4}$ m s^{-1}), forward time stepping did not lead to stationary solutions. Instead, periodic solutions with periods of order 1 yr were observed. Steady solutions obtained by directly solving (6), (7), and (8) turned out to be unstable with respect to small perturbations. On the $2° \times 1°$ grid the steady solutions become unstable at $\varepsilon \equiv 7 \times 10^{-8}$ s^{-1}. Such behavior is not unusual in hydrodynamic systems (Marcus 1981). The oscillating solutions do not reflect the actual behavior of the continuous system. We were always able to find a steady solution on a sufficiently fine grid, unless outcropping occurred. Higher resolution calculations also show that the steady solutions (in particular, the values of the transport) are increasingly less reliable as friction approaches the critical value where instability occurs. As in Krupitsky et al. (1996), very high resolution is required to retrieve correct values of the transport when closed characteristics are present. It appears to be necessary to resolve the internal boundary layers on both sides of the band of closed characteristics.

Experiments were also run for cases of stronger ($\alpha = 10$) and weaker ($\alpha = 0.1$) frictional coupling. The calculated transports are plotted in Fig. 1. The slopes of the curves in Fig. 1a vary between -0.85 and -0.95 (except in the high friction part of the case $\alpha = 10$, where it goes as $\varepsilon^{-2/3}$), consistent with the estimate of the previous section that slope is between $-\frac{5}{6}$ and -1. This means that interfacial pressure drag plays a progressively more important role in the momentum balance as friction decreases. The lower-layer transport, as expected, depends on friction very weakly (Fig. 1b). This result is consistent with the findings of Wolff (1990), who used a coarse resolution quasigeostrophic model and a narrower range of parameters.

Selected solutions for total streamfunction and interface displacement are presented in Figs. 2 and 3. It is clear that the topographic ridge (situated at 90°) exerts stronger influence on the flow than the trough (270°). The contours of ψ and h_1 are almost parallel except in the vicinity of the ridge and the trough, where the gradients of H vanish so that the JEBAR term vanishes.

As one expects from the arguments presented in the previous section, the circulations in the two layers in these solutions are decoupled. The upper-layer streamlines (which almost coincide with isolines of the total streamfunction ψ) are almost zonal, while the circulation in the lower layer mainly consists of weak closed gyres. The only difference between (7) and barotropic equation (11) of Krupitsky and Cane (1994) is the second term on the left of (7), JEBAR. Thus the JEBAR acts to insulate the upper layer from topography. This result is most readily understood in terms of the structure of the geostrophic contours in the upper layer using (14).

The degree of coupling between layers in this model depends on parameters g' and κ. As the barotropic limit ($g' \to 0$) is approached, the JEBAR term is certain to become negligible. Hence, as $g' \to 0$, the solution for ψ would approach that of Krupitsky and Cane (1994). Unfortunately, since the slope of the interface varies inversely with g' [cf. (3)], the numerical experiments at small g' require higher values of ε and κ to prevent outcropping of the lower layer near the poleward boundary or grounding of the upper layer at the equatorward boundary.

Therefore, we investigate coupling by increasing κ. The following scaling argument helps to understand the role of κ. Since the slope of the interface is to leading order determined by τ^x, f, and the friction coefficient μ [cf. (9)],

$$\frac{\partial h_1}{\partial y} \sim \frac{\tau^x f}{\mu}.$$

Assuming that ε is sufficiently small ($\alpha \gg 1$),

$$\frac{\partial h_1}{\partial y} \sim \frac{\tau^x f}{\kappa g'}.$$

The JEBAR term can make the solution to (7) substantially different from that in the barotropic case if

$$\frac{g'}{2} J\left(h_1^2, \frac{1}{H}\right) \gg \operatorname{curl}_z \frac{\tau}{H}.$$

This holds if

$$\kappa \ll \kappa_0 = H_1 f_0 \frac{L_y}{L_x} \frac{A}{H_0}.$$

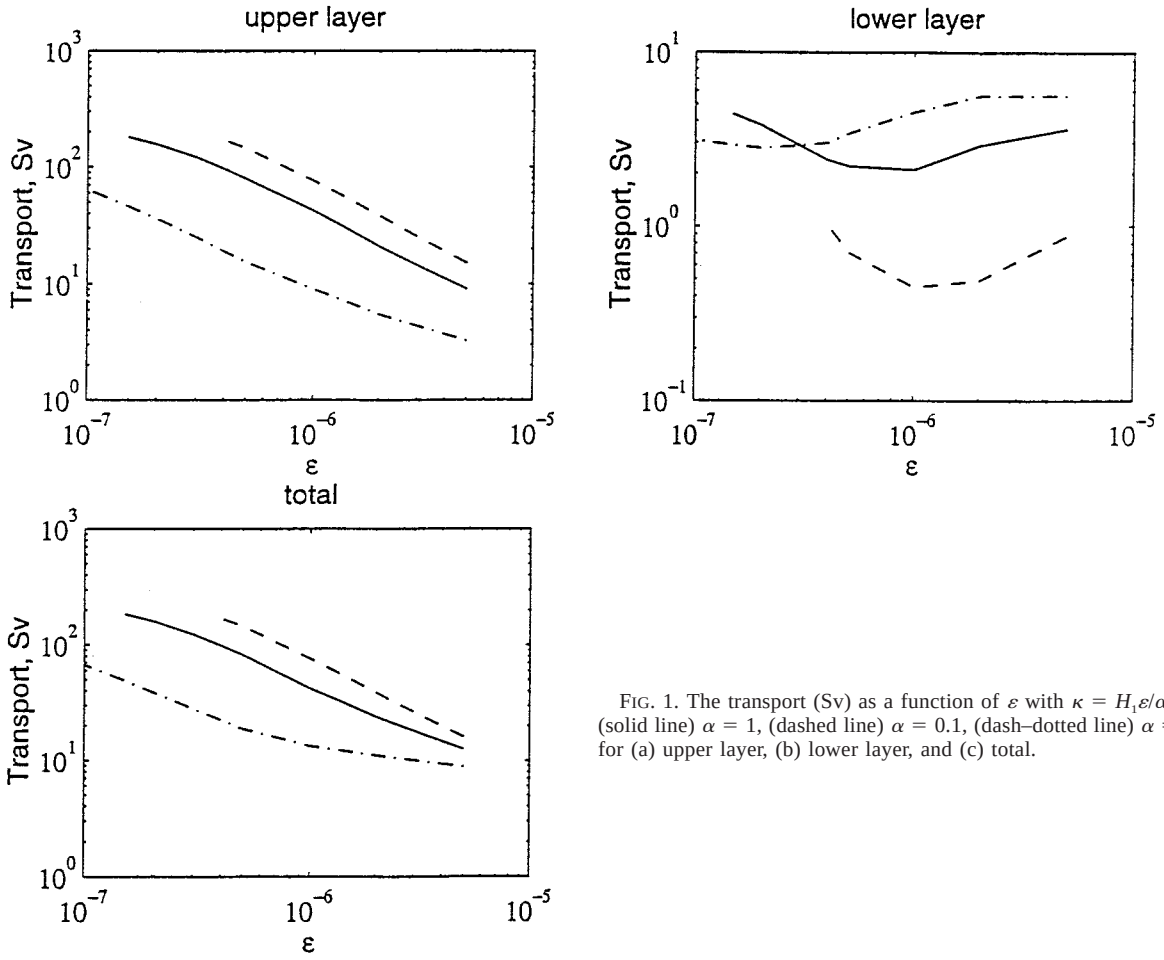

FIG. 1. The transport (Sv) as a function of ε with $\kappa = H_1\varepsilon/\alpha$ and (solid line) $\alpha = 1$, (dashed line) $\alpha = 0.1$, (dash–dotted line) $\alpha = 10$ for (a) upper layer, (b) lower layer, and (c) total.

With our choice of parameters $\kappa_0 \approx 3 \times 10^{-3}$ m s^{-1}. Figures 4 and 5 illustrate the evolution of ψ_1 and ψ_2 with increasing κ. With $\kappa = 10^{-3}$ m s^{-1}, the upper layer is barely affected by topography. With $\kappa = 10^{-2}$ m s^{-1}, JEBAR is about three times smaller than the wind forcing and the circulation patterns in the upper and the lower layers resemble each other. With $\kappa = 3 \times 10^{-2}$ m s^{-1}, the solution is almost barotropic. As is clear from Fig. 5, the lower-layer flow is dependent on κ only weakly: if T_1 varies as $\kappa^{-5/6}$, then total frictional drag on the lower layer κT_1 varies as $\kappa^{1/6}$. With sufficiently large κ this influence is passed to the upper layer via interfacial momentum exchange.

These results are in apparent contradiction with Killworth's (1992) theory predicting the self-similarity of the *inviscid* planetary geostrophic flow on density surfaces. However, the direct comparison with Killworth's arguments is difficult because his model does not include forcing explicitly. On the other hand, given the self-similarity of the time-mean velocity field in the ACC found in FRAM (Killworth 1992), our results are consistent with Killworth and Nanneh (1994), who find the balance between top and bottom drags in each (thin) isopycnal layer. Both in FRAM and in our model, self-similarity is associated with large vertical stresses. This suggests the possibility that the equivalent barotropic structure found by Killworth (1992) in FRAM is generated by interfacial stresses.

4. Conclusions

A theoretical and numerical analysis of a two-layer wind-driven channel model on a β plane, intended to simulate the ACC, shows that for a realistic range of parameters the regime most likely to be realized is the one suggested by Straub (1993): geostrophic contours in the upper layer are closed while those in the lower layer are blocked by solid boundaries. Then in the upper layer the momentum input from wind is balanced by lateral and interfacial friction and by interfacial pressure drag. The latter is shown to become progressively more important when coefficients of lateral and interfacial friction simultaneously decrease. In the lower layer, if lateral friction is sufficiently small, the momentum input from interfacial friction and from interfacial pressure drag is mainly balanced by topographic pressure drag.

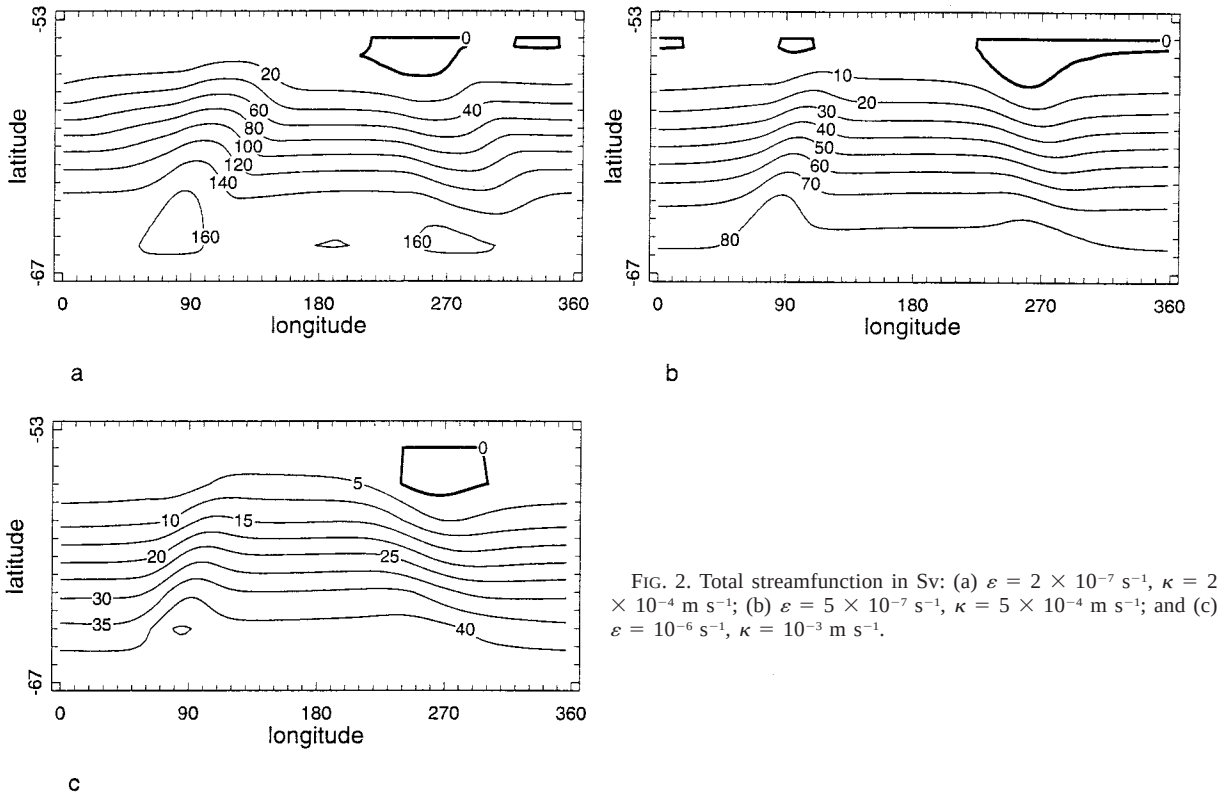

FIG. 2. Total streamfunction in Sv: (a) $\varepsilon = 2 \times 10^{-7}$ s^{-1}, $\kappa = 2 \times 10^{-4}$ m s^{-1}; (b) $\varepsilon = 5 \times 10^{-7}$ s^{-1}, $\kappa = 5 \times 10^{-4}$ m s^{-1}; and (c) $\varepsilon = 10^{-6}$ s^{-1}, $\kappa = 10^{-3}$ m s^{-1}.

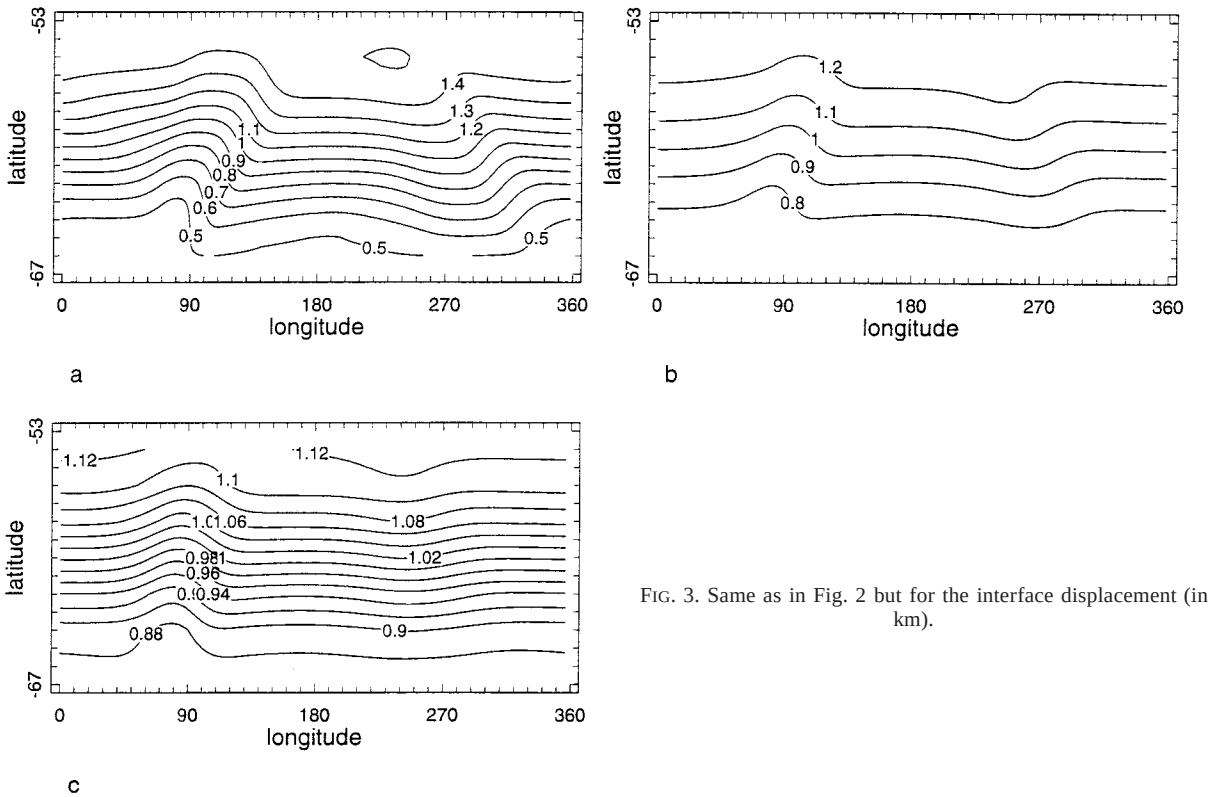

FIG. 3. Same as in Fig. 2 but for the interface displacement (in km).

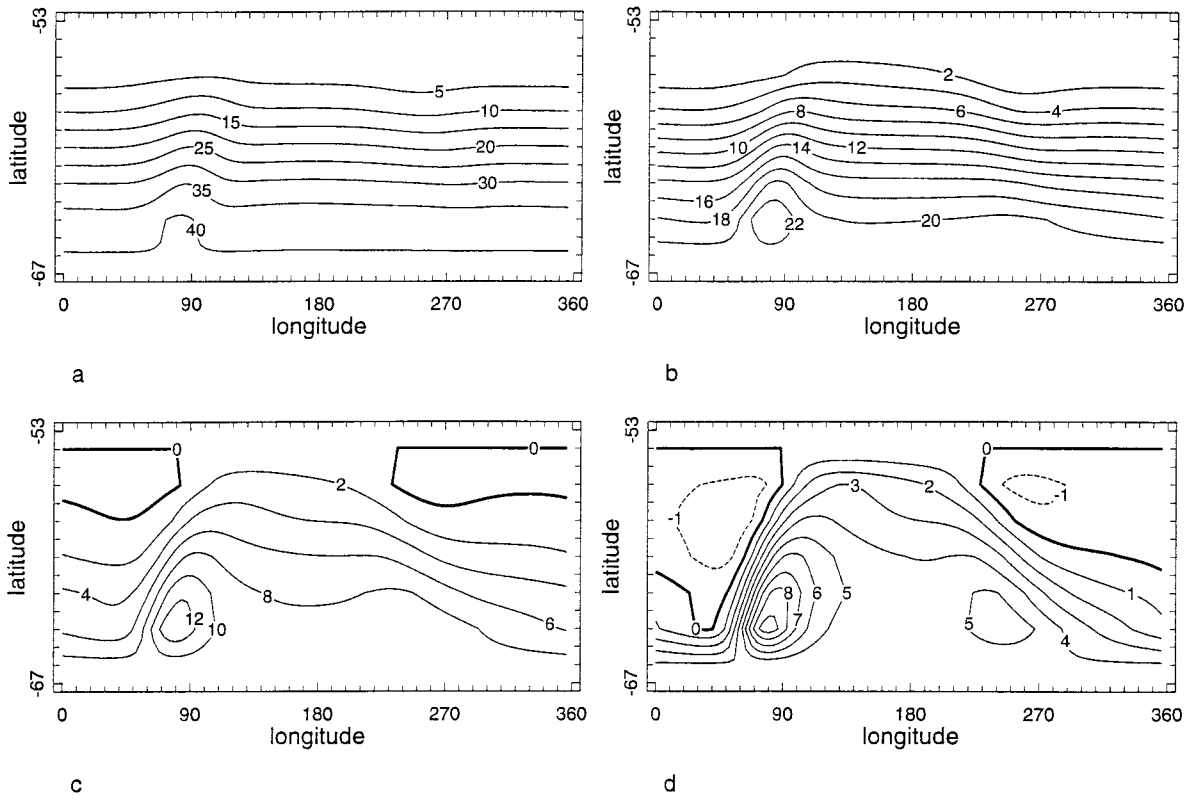

FIG. 4. Upper-layer streamfunction ψ_1 with $\varepsilon = 10^{-4}$ s^{-1}: (a) $\kappa = 10^{-3}$ m s^{-1}, (b) $\kappa_0 \approx 3 \times 10^{-3}$ m s^{-1}, (c) $\kappa = 10^{-2}$ m s^{-1}, and (d) $\kappa = 3 \times 10^{-2}$ m s^{-1}.

Thus, in the total budget the momentum input by the wind is balanced by the upper-layer lateral friction and by topographic pressure drag. Their relative importance in this model is determined by the ratio of lateral friction to interfacial friction in the upper layer. Interpreting the interfacial friction as a surrogate for the eddy activity puts this analysis in general agreement with results of eddy-resolving experiments (McWilliams et al. 1978; Wolff and Olbers 1989; Treguier and McWilliams 1990; Wolff et al. 1990; Wolff et al. 1991).

In contrast to the barotropic models of Krupitsky and Cane (1994) or Krupitsky (1995), here we find unrestricted (except by outcropping) growth of the upper-layer (and therefore total) transport. We conclude that topographic pressure forces, again unlike those in barotropic models, may not be sufficiently large to effectively restrict the total transport. Instead, the effectiveness of topographic control depends on the magnitude of the vertical momentum exchange. In the real ocean as the flow speeds up, more eddies are generated, so momentum exchange increases. This effect is not included in our study, but increasing κ allows our model to indicate how it might work. As a step toward greater realism, we could set κ to be a function of shear. Interpreting the numerical models in this framework leads us to suggest that their transports are too high because their effective interfacial friction and pressure drag are too weak. Since the interfacial effects in these models are largely the result of baroclinic eddies, we are led to suggest that the level of eddy activity is too low in these models.

The rate of growth of the upper-layer transport T_1 varies between ε^{-1} and $\varepsilon^{-5/6}$ as lateral and interfacial friction simultaneously decrease (cf. Fig. 1). This theoretical estimate is confirmed by numerical experiments. The magnitude of the total transport depends strongly on the efficiency of the momentum transfer from the upper to the lower layer, that is, on the ratio κ/ε.

These results are in contrast to Wang (1993), who found a finite limit to the transport by assuming that excessive shear is removed by an implicit baroclinic instability. It is this assumption that effectively imposes the ''inviscid'' limit in his calculation. We do not have such a limiting mechanism in our model. Instead, the eddies are parameterized by interfacial and lateral friction. It is possible that baroclinic instability occurs in planetary geostrophic systems, despite the absence of the nonlinear terms. [Colin de Verdiere (1986) shows it for a three-layer flat bottom model with no barotropic mode.] In our calculations, however, it does not happen.

In most numerical experiments the circulations in the two layers are decoupled. The decoupling can be explained by the JEBAR term, whose magnitude decreases as interfacial friction increases. The solution tends to

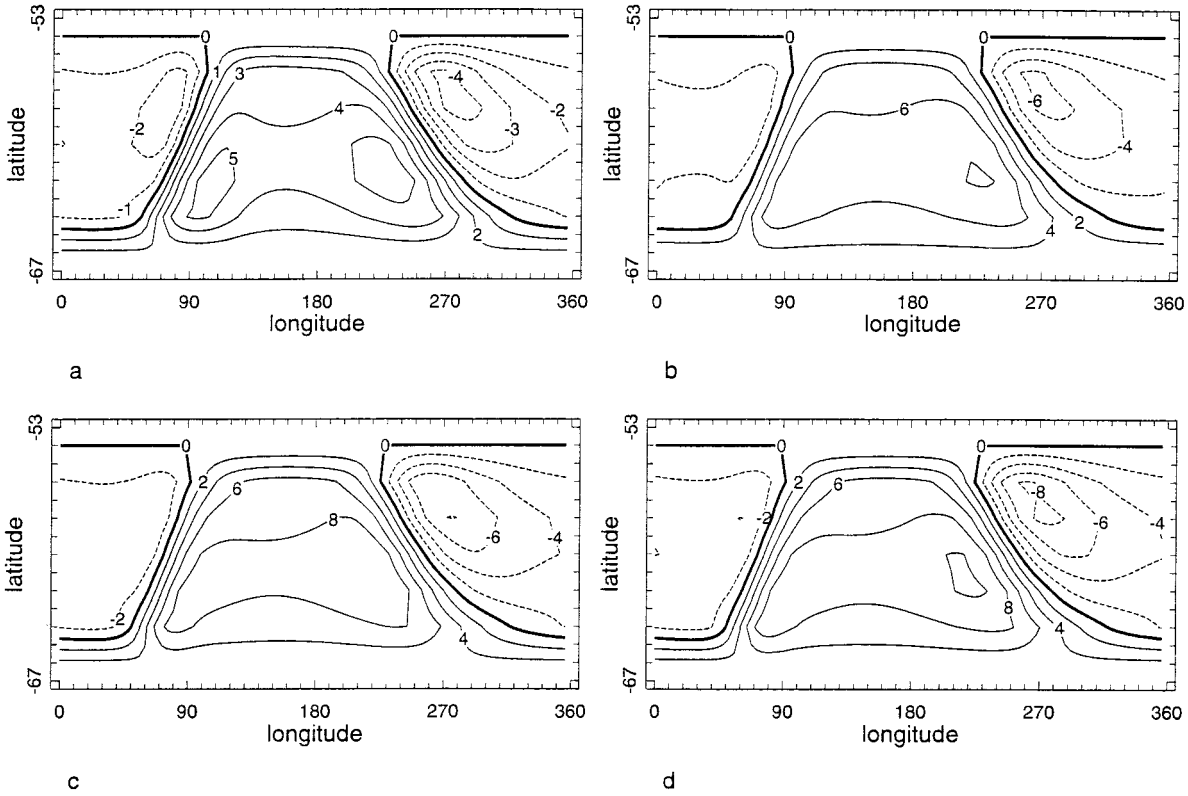

FIG. 5. Same as Fig. 4 but for the lower layer streamfunction ψ_2.

the barotropic one if the interfacial friction is sufficiently large to render the JEBAR term to be of the same order or less than the wind-stress curl term in the potential vorticty equation. A critical value of interfacial friction separating coupled and uncoupled regimes is determined. It depends on the size and scale of the topography and on the scale of the wind stress, but not on the wind amplitude.

Acknowledgments. The authors appreciate discussions with Vladimir Kamenkovich, Alexey Kaplan, and Naftali Tsitverblit. Thoughtful comments of the two anonymous reviewers helped clarify the presentation. This work was supported by NOAA Grant NA 37GP0518.

REFERENCES

Colin de Verdiere, A., 1986: On mean flow instabilities within the planetary geostrophic equations. *J. Phys. Oceanogr.,* **16,** 1981–1984.

Cox, M. D., 1975: A baroclinic numerical model of World Ocean: preliminary results. *Proc. Symp. on Numerical Models of Ocean Circulation,* Washington, DC, Natl. Acad. Sci., 107–120.

FRAM Group, 1991: An eddy-resolving model of the Southern Ocean. *Eos Trans. Amer. Geophys. Union,* **72,** 169–175.

Gordon, A. L., E. Molinelli, and T. Baker, 1978: Large-scale relative dynamic topography in the Southern Ocean. *J. Geophys. Res.,* **83** (C6), 3023–3032.

Grose, T. J., J. A. Johnson, and G. R. Bigg, 1995: A comparison between the FRAM (Fine Resolution Antarctic Model) results and observations in the Drake Passage. *Deep-Sea Res.,* **42,** 365–388.

Harrison, D. E., 1979: Eddies and the general circulation of numerical model gyres: An energetic prospective. *Rev. Geophys. Space Phys.,* **5,** 969–979.

Johnson, J. A., and R. B. Hill, 1975: A three-dimensional model of the Southern Ocean with bottom topography. *Deep-Sea Res.,* **22,** 745–751.

Kamenkovich, V. M., 1960: The influence of bottom relief on the Antarctic Circumpolar Current. (Translated from Russian). *Dokl. Akad. Nauk SSSR,* **134,** 983–984.

——, 1962: On the theory of the Antarctic Circumpolar Current. (Translated from Russian). *Tr. Inst. Okeanol.,* **56,** 245–306.

Killworth, P. D., 1992: An equivalent-barotropic mode in the Fine Resolution Antarctic model. *J. Phys. Oceanogr.,* **22,** 1379–1387.

——, and M. M. Nanneh, 1994: Isopycnal momentum budget of the Antarctic Circumpolar Current in the fine resolution Antarctic model. *J. Phys. Oceanogr.,* **24,** 1201–1223.

Krupitsky, A., 1995: Local and remote forcing of the barotropic transport through a periodic gap in a basin with bottom topography. *J. Mar. Res.,* **53,** 201–210.

——, and M. A. Cane, 1994: On topographic pressure drag in a zonal channel. *J. Mar. Res.,* **52,** 1–22.

——, V. M. Kamenkovich, N. Naik, and M. A. Cane, 1996: A linear equivalent barotropic model of the A ntarctic Circumpolar Current with realistic coastlines and bottom topography. *J. Phys. Oceanogr.,* **26,** 1803–1824.

Marcus, P. S., 1981: Effects of truncation in modal representations of thermal convection. *J. Fluid Mech.,* **103,** 241–255.

Marshall, D., 1995: Topographic steering of the Antarctic Circumpolar Current. *J. Phys. Oceanogr.,* **25,** 1636–1650.

McWilliams, J. C., W. R. Holland, and J. H. S. Chow, 1978: A description of numerical Antarctic Circumpolar Currents. *Dyn. Atmos. Oceans,* **2,** 213–291.

Mertz, G., and D. G. Wright, 1992: Interpretations of the JEBAR term. *J. Phys. Oceanogr.*, **22,** 301–305.

Salmon, R., 1992: A two-layer Gulf Stream over a continental slope. *J. Mar. Res.*, **50,** 341–365.

Sarkisyan, A. S., and V. F. Ivanov, 1971: Joint effect of baroclinicity and bottom relief as an important factor in the dynamics of sea currents. (Translated from Russian), *Izv. Acad. Sci. USSR Atmos. Oceanic Phys.*, **7** (2), 173–188.

Straub, D. N., 1993: On the transport and angular momentum balance of channel models of the Antarctic Circumpolar Current. *J. Phys. Oceanogr.*, **23,** 776–782.

Treguier, A. M., and J. C. McWilliams, 1990: Topographic influences on wind-driven, stratified flow in a β-plane channel: An idealized model for the Antarctic Circumpolar Current. *J. Phys. Oceanogr.*, **20,** 321–343.

Wang, L., 1993: The dynamic role of ridges in a β-plane. Ph.D. thesis, MIT-WHOI Joint Program, 251 pp. [Available from Dept. of Education, WHOI, Woods Hole, MA 02543.]

——, 1994: A linear homogeneous channel model for topographic control of the Antarctic Circumpolar Current. *J. Mar. Res.*, **52,** 649–685.

——, and R. X. Huang, 1995: A linear homogeneous model of wind-driven circulation in a β-plane channel. *J. Phys. Oceanogr.*, **25,** 587–603.

Wolff, J.-O., 1990: Zur Dynamik des Antarktischen Zirkumpolarstromes. Dissertation am Fachbereich Geowissenschaften der Universität Hamburg, Examensarbeit Nr. 2, Max-Plank-Institut für Meteorologie, 142 pp. [P thesis in German), ISSN 0938-5177.]

——, and D. J. Olbers, 1989: The dynamical balance of the Antarctic Circumpolar Current studied with an eddy resolving quasi-geostrophic model. *Mesoscale-Synoptic Coherent Structures in Geophysical Turbulence*, J. C. J. Nihoul and B. M. Jamart, Eds., Elsevier, 435–458.

——, V. O. Ivchenko, A. V. Klepikov, and D. J. Olbers, 1990: On the effects of topography on the dynamics of zonal currents in the ocean. (Translated from Russian). Dokl. *Akad. Nauk SSSR*, **313,** 323–327.

——, E. Maier-Reimer, and D. J. Olbers, 1991: Wind-driven flow over topography in a zonal β-plane channel: A quasi-geostrophic model of the Antarctic Circumpolar Current. *J. Phys. Oceanogr.*, **21,** 236–264.